catalysts

MDPI

Article

# "Storage-Discharge" Ethanol Cold Plasma for Synthesizing High Performance $Pd/Al_2O_3$ Catalysts

**Hongyang Wang, Tengda Zhang, Yufa Zhou, Xiuling Zhang * and Lanbo Di ***

College of Physical Science and Technology, Dalian University, Dalian 116622, China; hywang68@sina.com (H.W.); tdzhang2258@163.com (T.Z.); zhouyufa1013@163.com (Y.Z.)

* Correspondence: zhangxiuling@dlu.edu.cn (X.Z.); dilanbo@dlu.edu.cn (L.D.); Tel.: +86-411-8740-2712 (X.Z. & L.D.)

Received: 17 July 2020; Accepted: 6 August 2020; Published: 8 August 2020


**Abstract:** Atmospheric pressure cold plasma is an environmentally friendly and novel method to synthesize supported metal catalysts, which usually uses active hydrogen species to reduce metal ions. Ethanol is a hydrogen-rich renewable liquid hydrogen source, and it is more convenient to store and transport than $H_2$. In this study, a "storage-discharge" ethanol cold plasma was used to prepare $Pd/Al_2O_3$-EP catalysts, and the obtained catalysts are used for CO oxidation. The complete oxidation of CO temperature ($T_{100}$) over $Pd/Al_2O_3$-EP was 145 °C, which was comparable to the performance of $Pd/Al_2O_3$-HP that was synthesized by atmospheric pressure hydrogen cold plasma. $Pd/Al_2O_3$-EP-C obtained by calcining $Pd/Al_2O_3$-EP at 450 °C for 2 h in air atmosphere in order to remove residual carbon species showed much higher CO oxidation activity, and $T_{100}$ was 130 °C. The $Pd/Al_2O_3$ catalysts were characterized by X-ray diffraction (XRD), X-ray photoelectron diffraction (XPS), Brunauer–Emmett–Teller (BET), and transmission electron microscopy (TEM), and the structure-performance relationship was analyzed. The results indicate that the "storage-discharge" ethanol cold plasma can reduce the Pd precursor ions into metallic Pd state, and the dissociation of ethanol forms lots of highly active chemisorbed oxygen species, which can enhance the performance of $Pd/Al_2O_3$-EP for CO oxidation. In contrast, $Pd/Al_2O_3$-EP-C shows much higher CO oxidation activity, which is mainly attributed to the removal of the residual carbon species, and the exposure of more Pd active sites and chemisorbed oxygen species. The "storage-discharge" ethanol cold plasma is a safe and efficient novel method for synthesizing supported Pd catalysts, and it has important potential for the preparation and application of supported metal catalysts.

**Keywords:** dielectric barrier discharge (DBD); storage-discharge; ethanol plasma; Pd; CO oxidation

## 1. Introduction

Atmospheric pressure (AP) cold plasma has gained increasing attention in the preparation of supported metal catalysts. AP cold plasma has low electron energy, so it is required to add hydrogen-containing gases ($H_2$, $NH_3$, etc.) into the working gas. The metal ions can be reduced by the active hydrogen species generated by the hydrogen-containing gases during the discharge plasma [1–4]. When compared to low pressure (LP) cold plasma, the active hydrogen species in AP cold plasma demonstrate a much stronger reduction ability and lower preparation cost without using the sophisticated and expensive vacuum system [5]. AP hydrogen cold plasma is widely used in the synthesis of supported metal catalysts [2,6,7], but the gaseous hydrogen has caused severe storage and transportation problem. Ethanol, as a potential liquid hydrogen carrier, exhibits superiority in high catalytic energy density, high calorific value, non-toxicity, easy storage, and strong practicability. It has become a hot spot for researchers to study hydrogen production from liquid fuel [8–11].

Various technologies have been applied to produce hydrogen from ethanol reforming, such as steam-reforming, catalytic reforming, and water electrolysis. However, these technologies have certain limitations. For example, steam-reforming demands high temperatures, catalytic reforming requires high-efficiency catalyst assistance, and water electrolysis needs high energy cost for hydrogen production. As a fast, simple, and green method, hydrogen production by ethanol reforming using plasma shows many advantages. Zhou et al. [12] employed non-thermal spark plasma discharges to rapidly and selectively reform ethanol at low temperature (<40 °C) without using a catalyst. By using this method, ethanol was effectively reformed into $H_2$ with a high $H_2$ yield ($H_2$ content > 90%) at a low energy consumption (~0.96 kWh·m$^{-3}$ $H_2$). Meanwhile, valuable carbon dots (CDs) were also generated during the ethanol reforming process. Ulejczyk et al. [13] used dielectric barrier discharge (DBD) in order to produce hydrogen from a mixture of water and ethanol. The results showed that the conversion of ethanol was 71%. The cooling-off gas consisted 48–56% hydrogen and 17–21% carbon monoxide, and the energy yield of hydrogen production can reach 6.15 mol$H_2$·kWh$^{-1}$. When compared to the catalytic reforming of ethanol method, the application of plasma can avoid the deposition of soot on the catalyst, which may reduce the reforming efficiency. Bardos et al. [14] obtained hydrogen-rich syngas through immersing a pulsed DC discharge plasma in ethanol and water mixtures. The results showed that a syngas with 60% hydrogen can be generated at 250 sccm outflow rate, corresponding to a hydrogen production efficiency of 12 kWh·kg$^{-1}$ $H_2$. In addition, liquid pulse discharge, which combines the advantages of pulse discharge and liquid phase discharge, was also employed to reduce the energy consumption of hydrogen production. Xin et al. [15] adopted pulsed spark discharge with needle-balls configuration to produce hydrogen from ethanol-water mixtures. The results proved that when the pulse discharge voltage peak is 30 kV, the hydrogen flow rate can reach 1100 mL·min$^{-1}$ with the energy yield of 141.3 g$H_2$·kWh$^{-1}$. The above researches have shown that ethanol reforming by plasma to produce hydrogen has important application value. Based on this, Di et al. [1] developed an AP DBD cold plasma method while using ethanol as the source of active hydrogen species to treat a Pd/P25 precursor to prepare Pd/P25-EP. The Pd/P25-EP catalyst was further calcined in an air atmosphere at 300 °C for 2 h to removal the residual carbon species formed by ethanol dissociation in cold plasma, and it was recorded as Pd/P25-EP-C. The results illustrated that, when the reaction temperature was 120 °C, the turn over frequency (TOF) value of Pd/P25-EP-C is 3.1 times as that of the Pd/P25-HP synthesized by hydrogen cold plasma. However, the performance of the as-prepared Pd/P25-EP is poor. Di et al. [16] further adopted the successive AP ethanol cold plasma to synthesize Pd/C catalysts. The results indicated that excessive residual carbon species may inhibit CO oxidation over the catalyst. Therefore, if a "storage-discharge" ethanol cold plasma method instead of the successive method can be developed and employed to synthesize supported metal catalysts, it will be competitive.

The "storage-discharge" method has been used in the preparation of catalysts and the removal of volatile organic compounds (VOCs). Zhang et al. [17] prepared a supported $TiO_2$/γ-$Al_2O_3$ photocatalyst using a cyclic "adsorption-discharge" method. During the process, $TiCl_4$ was adsorbed on the γ-$Al_2O_3$ pellets and then subjected to plasma treatment. The obtained $TiO_2$/γ-$Al_2O_3$ photocatalyst showed stronger adhesion to the support, as compared with conventional plasma chemical vapor deposition. In addition, the "storage-discharge" process has also widely used for removing VOCs [18–23]. The VOCs can be effectively removed by the synergy of the packed catalysts and the plasma. In addition, when compared with the continuous discharge process, "storage-discharge" can significantly reduce energy consumption.

In this work, Pd/$Al_2O_3$ catalysts for CO oxidation application were synthesized by a "storage-discharge" ethanol cold plasma method, and the structure-performance relationship was discussed. The Pd/$Al_2O_3$-EP that was prepared by "storage-discharge" ethanol cold plasma and Pd/$Al_2O_3$-HP synthesized by AP hydrogen cold plasma exhibited similar performance for CO oxidation, and 100% CO conversion temperature ($T_{100}$) over them was 145 °C. Pd/$Al_2O_3$-EP shows high CO catalytic oxidation activity, mainly attributed to the fact that the "storage-discharge" ethanol cold

plasma can reduce the Pd precursor ions into metallic Pd, and much chemisorbed oxygen species were formed by ethanol dissociation. Pd/$Al_2O_3$-EP-C was further obtained by calcining Pd/$Al_2O_3$-EP at 450 °C for 2 h. More Pd active sites and chemisorbed oxygen species, beneficial to CO oxidation, are exposed and formed due to the thermal removal of the residual carbon species. Therefore, Pd/$Al_2O_3$-EP-C exhibits much higher performance for CO oxidation and $T_{100}$ was decreased to 130 °C.

## 2. Results and Discussion

Figure 1 illustrates the X-ray diffraction (XRD) patterns of Pd/$Al_2O_3$-EP, Pd/$Al_2O_3$-EP-C, Pd/$Al_2O_3$-HP, and $Al_2O_3$ support. There are four characteristic diffraction peaks of $Al_2O_3$ support at 32.8°, 37.3°, 45.9°, and 67.2°, as shown in Figure 1 (JCPDS No. 04-0877). As a result of the covering effect of Pd species, the characteristic diffraction peaks of $Al_2O_3$ support in Pd/$Al_2O_3$-EP, Pd/$Al_2O_3$-EP-C, and Pd/$Al_2O_3$-HP are reduced to some extent. It can be seen from the XRD patterns of Pd/$Al_2O_3$-EP, Pd/$Al_2O_3$-EP-C and Pd/$Al_2O_3$-HP that there is no obvious characteristic diffraction peak of metal Pd, which may be ascribed to the high dispersion of Pd nanoparticles on the surface of the $Al_2O_3$ support [24–27] and (or) the low Pd content of the samples [28]. The XRD pattern of Pd/$Al_2O_3$-EP-C shows three diffraction peaks at 33.9°, 41.9°, and 54.8°, corresponding to the (101), (110), and (111) crystal planes the tetragonal PdO structure (JCPDS No. 41-1107), which is in line with the transmission electron microscopy (TEM) results (Figure 2). It suggests that some oxidized Pd species in Pd/$Al_2O_3$-EP-C are formed due to the calcination at high temperature in air atmosphere. Baylet et al. also observed a similar phenomenon [29].

Figure 2 illustrates the TEM images and histograms of the size distribution of Pd/$Al_2O_3$-EP, Pd/$Al_2O_3$-EP-C, and Pd/$Al_2O_3$-HP, and Table 1 summarizes the relevant data. The Pd nanoparticles in Pd/$Al_2O_3$-EP and Pd/$Al_2O_3$-HP show high dispersion on the $Al_2O_3$ support, as shown in Figure 2. It can be seen from Table 1 that the Pd nanoparticles average sizes ($D_{mean}$) in Pd/$Al_2O_3$-EP, Pd/$Al_2O_3$-EP-C, and Pd/$Al_2O_3$-HP are 3.2 ± 0.4, 3.7 ± 0.6, and 3.0 ± 0.5 nm, respectively. The calcination process at 450 °C under air atmosphere is the main reason for the increase of the Pd nanoparticles size in Pd/$Al_2O_3$-EP-C. From the images obtained by HRTEM, it can be seen that all the Pd/$Al_2O_3$-EP, Pd/$Al_2O_3$-EP-C, and Pd/$Al_2O_3$-HP contain Pd(111) crystal planes corresponding to the face-centered cubic structure with the interplanar spacing of 0.225 nm. In addition, Pd/$Al_2O_3$-EP-C contains PdO(101) crystal plane with the interplanar spacing of 0.265 nm. The HRTEM of Pd/$Al_2O_3$-EP-C shows that there are many mismatch dislocations that are caused by stress at the junction of Pd(111) and PdO(101) crystal planes, and the lattice mismatch degree is 17.8%. Zhang et al. [30] claimed that the surface oxidation of Pd nanoparticles started from the edge sites that have atomic steps or vertices, exhibiting a crystallography preference that proceeded faster on Pd(111) surface.

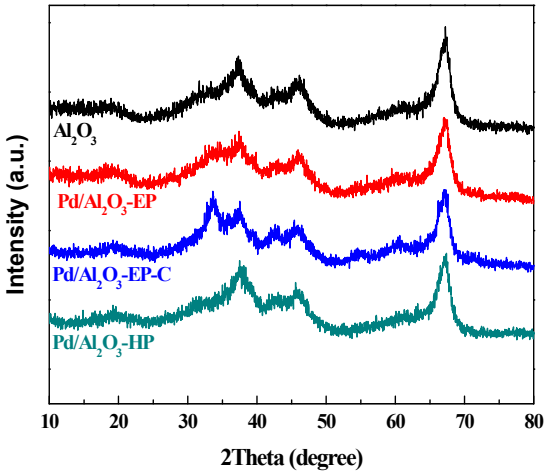


**Figure 1.** X-ray diffraction (XRD) patterns of Pd/$Al_2O_3$-EP, Pd/$Al_2O_3$-EP-C, Pd/$Al_2O_3$-HP, and the $Al_2O_3$ support.

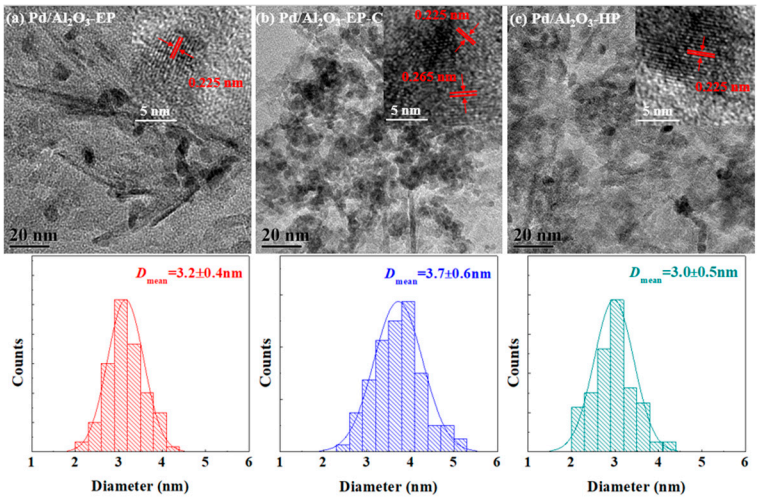


**Figure 2.** Transmission electron microscopy (TEM) images of (**a**) Pd/$Al_2O_3$-EP, (**b**) Pd/$Al_2O_3$-EP-C, (**c**) Pd/$Al_2O_3$-HP, and the corresponding histograms of size distributions of the Pd nanoparticles and HRTEM images (insets).

**Table 1.** Brunauer–Emmett–Teller (BET) results of the $Al_2O_3$ support, Pd/$Al_2O_3$-EP, Pd/$Al_2O_3$-EP-C, and Pd/$Al_2O_3$-HP.

| Sample | $S_{BET}$ ($m^2 \cdot g^{-1}$) | $V_p$ ($cm^3 \cdot g^{-1}$) | $D_p$ (nm) | $D_{Pd}$ (nm) |
|---|---|---|---|---|
| $Al_2O_3$ | 196.0 | 0.508 | 7.92 | |
| Pd/$Al_2O_3$-EP | 203.8 | 0.434 | 7.92 | 3.2 |
| Pd/$Al_2O_3$-EP-C | 187.8 | 0.471 | 7.90 | 3.7 |
| Pd/$Al_2O_3$-HP | 196.3 | 0.438 | 7.94 | 3.0 |

$N_2$ adsorption–desorption characterization analysis was adopted to explore the porous structure of $Al_2O_3$, Pd/$Al_2O_3$-EP, Pd/$Al_2O_3$-EP-C, and Pd/$Al_2O_3$-HP. The $N_2$ adsorption–desorption isotherms and the corresponding pore size distributions curves of $Al_2O_3$ and the Pd/$Al_2O_3$ catalysts are presented in Figure S1. The Brunauer–Emmett–Teller (BET) specific surfaces areas ($S_{BET}$), pore volumes ($V_p$), and pore sizes ($D_p$) distributions of the samples are summarized in Table 1. The $S_{BET}$ of the samples follows the order: Pd/$Al_2O_3$-EP > Pd/$Al_2O_3$-HP > Pd/$Al_2O_3$-EP-C, and the corresponding data are 203.8, 196.3, and 187.8 $m^2 \cdot g^{-1}$, respectively (Figure S1 and Table 1). When compared with $Al_2O_3$ support, the $S_{BET}$ of Pd/$Al_2O_3$-EP synthesized by "storage-discharge" ethanol cold plasma is slightly increased, which may be attributed to the carbon deposits dissociated from ethanol during cold plasma. In contrast, the $S_{BET}$ of Pd/$Al_2O_3$-EP-C obtained by calcining Pd/$Al_2O_3$-EP was reduced to 187.8 $m^2 \cdot g^{-1}$, which is mainly due to the burn-up of the porous structure formed by carbon during the high-temperature calcination process. The $V_p$ of Pd/$Al_2O_3$-EP-C is 0.471 $cm^3 \cdot g^{-1}$, which is slightly larger than that of Pd/$Al_2O_3$-EP (0.434 $cm^3 \cdot g^{-1}$) and Pd/$Al_2O_3$-HP (0.438 $cm^3 \cdot g^{-1}$), attributed to the removal of the residual carbon species by calcination treatment. Moreover, there is no too much difference in $D_p$ among the samples.

Figure 3 presents the X-ray photoelectron diffraction (XPS) spectra of Pd3d, O1s and C1s in Pd/$Al_2O_3$-EP, Pd/$Al_2O_3$-EP-C, and Pd/$Al_2O_3$-HP. There are two characteristic peaks identified at 335.3 and 336.6 eV by deconvoluting the peaks of $Pd3d_{5/2}$, corresponding to $Pd^0$ and $Pd^{2+}$ [31], respectively, as shown in Figure 3a. The relative percentage of Pd components and Pd/Al atomic ratios in Pd/$Al_2O_3$ catalysts were calculated according to the surfaces of the peak areas, and illustrated in Table 2. As shown in Table 2, the $Pd^0$ contents in Pd/$Al_2O_3$-EP, Pd/$Al_2O_3$-EP-C, and Pd/$Al_2O_3$-HP are 95.6%, 54.9%, and 98.8%, respectively. The high and similar metallic $Pd^0$ content in Pd/$Al_2O_3$-EP and Pd/$Al_2O_3$-HP proves that "storage-discharge" ethanol plasma has the ability to reduce Pd precursor ions to a metallic state, like hydrogen plasma. In addition, the $Pd^{2+}$ contents in Pd/$Al_2O_3$-EP, Pd/$Al_2O_3$-EP-C, and Pd/$Al_2O_3$-HP are 4.4%, 45.1%, and 1.2%, respectively. The $Pd^{2+}$ content in Pd/$Al_2O_3$-EP-C obtained

by calcining $Pd/Al_2O_3$-EP is increased to 45.1%, suggesting that some metallic Pd in $Pd/Al_2O_3$-EP are oxidized at 450 °C for 2 h in air atmosphere. This is consistent with the XRD results (Figure 1). The atomic ratios of Pd/Al in $Pd/Al_2O_3$-EP, $Pd/Al_2O_3$-EP-C, and $Pd/Al_2O_3$-HP are 0.0128, 0.0248, and 0.0229, respectively. The Pd/Al atomic ratio of $Pd/Al_2O_3$-EP is the smallest among the three samples, which is mainly attributed to the coverage of the residual carbon species dissociated from ethanol during the "storage-discharge" ethanol cold plasma process. After the calcination treatment, the residual carbon species were removed, and the Pd/Al atomic ratio of $Pd/Al_2O_3$-EP-C increases to 0.0248, revealing that more active sites are exposed.

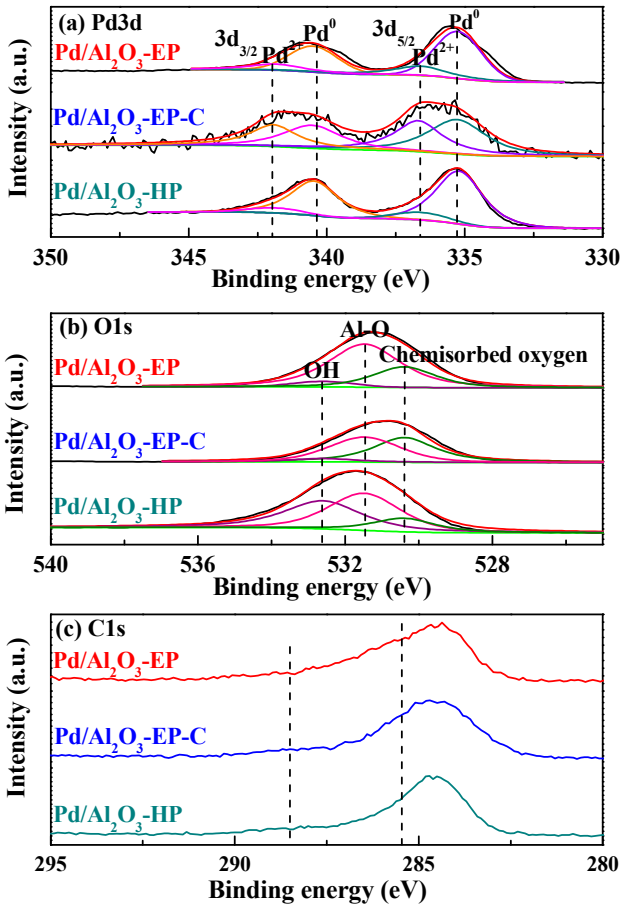


**Figure 3.** X-ray photoelectron diffraction (XPS) spectra of (**a**) Pd3d, (**b**) O1s, (**c**) C1s in $Pd/Al_2O_3$-EP, $Pd/Al_2O_3$-EP-C, and $Pd/Al_2O_3$-HP.

**Table 2.** The Pd component content, Pd/Al atomic ratios and the ratios of chemisorbed oxygen species in O1s ($O_{chem}$%) for the $Pd/Al_2O_3$ samples.

| Sample | Pd Composition (%) | | Pd/Al | $O_{chem}$ % |
|---|---|---|---|---|
| | $Pd^0$ | $Pd^{2+}$ | | |
| $Pd/Al_2O_3$-EP | 95.6 | 4.4 | 0.0128 | 27.2 |
| $Pd/Al_2O_3$-EP-C | 54.9 | 45.1 | 0.0248 | 46.9 |
| $Pd/Al_2O_3$-HP | 98.8 | 1.2 | 0.0229 | 15.3 |

Figure 3b illustrates the O1s XPS spectra of $Pd/Al_2O_3$-EP, $Pd/Al_2O_3$-EP-C, and $Pd/Al_2O_3$-HP. All of them can be fitted with three characteristic peaks at 532.6, 531.5, and 530.4 eV, ascribing to -OH [32], Al-O [24] and chemisorbed oxygen [25], respectively. Moreover, it can be seen from Table 2 that the chemisorbed oxygen contents in $Pd/Al_2O_3$-EP, $Pd/Al_2O_3$-EP-C, and $Pd/Al_2O_3$-HP are 27.2%, 46.9%, and 15.3%, respectively. Because oxygen-containing $Pd(NO_3)_2$ is used as the Pd precursor to synthesize

the $Pd/Al_2O_3$ catalysts, some chemisorbed oxygen can be formed and detected on the surface of the $Al_2O_3$ support [25]. Chemisorbed oxygen species are beneficial to promoting CO oxidation [33]. $Pd/Al_2O_3$-EP presents more highly active chemisorbed oxygen species (27.2%) than $Pd/Al_2O_3$-HP (15.3%), which is ascribed to the dissociation of ethanol during the preparation process to produce. As for $Pd/Al_2O_3$-EP-C, prepared by calcination of $Pd/Al_2O_3$-EP at 450 °C for 2 h, the residual carbon species are removed, and more chemisorbed oxygen species are exposed. Therefore, the content of chemisorbed oxygen in $Pd/Al_2O_3$-EP-C is increased to 46.9%.

Ethanol dissociation in cold plasma can not only generate active reducing species, but can also generate carbon species [1,27]. The C1s XPS of the three samples were analyzed to study the generation and removal of the carbon species. When compared to $Pd/Al_2O_3$-HP, the intensity of C1s XPS spectrum for $Pd/Al_2O_3$-EP is stronger, as shown in Figure 3c. Two curves at 288.5 and 285.5 eV can be fitted with the C1s XPS spectrum in $Pd/Al_2O_3$-EP, ascribing to the C-O [34] and amorphous carbon species [35] derived from ethanol dissociation in cold plasma. As far as $Pd/Al_2O_3$-EP-C is concerned, the intensity of the two peaks are decreased, revealing that the calcination process can remove the residual carbon species, which is in line with the TG/DTG results (Figure S2).

The $Pd/Al_2O_3$-HP sample that was prepared by AP hydrogen cold plasma was adopted as a reference to explore the "storage-discharge" ethanol cold plasma on the performance of $Pd/Al_2O_3$ catalysts. The catalytic performance for CO oxidation of $Pd/Al_2O_3$-EP, $Pd/Al_2O_3$-EP-C, and $Pd/Al_2O_3$-HP catalysts were evaluated, and the reaction temperature ranged from 30 to 160 °C, as shown in Figure 4. It can be observed that the CO conversion of three $Pd/Al_2O_3$ catalysts gradually increased with the increase of reaction temperature. $Pd/Al_2O_3$-EP and $Pd/Al_2O_3$-HP exhibit similar CO catalytic oxidation activity, and both the 100% CO conversion temperature ($T_{100}$) are achieved at 145 °C. The TEM results indicate that the particle sizes of $Pd/Al_2O_3$-EP (3.2 nm) and $Pd/Al_2O_3$-HP (3.0 nm) are similar. The Pd/Al atomic ratio of $Pd/Al_2O_3$-HP (0.0229) is higher than that of $Pd/Al_2O_3$-EP (0.0128), while $Pd/Al_2O_3$-EP has more active chemisorbed oxygen species (27.2%) derived from ethanol than that in $Pd/Al_2O_3$-HP (15.3%). Therefore, $Pd/Al_2O_3$-EP and $Pd/Al_2O_3$-HP show similar catalytic performance. In contrast, the $T_{100}$ of $Pd/Al_2O_3$-EP-C that was obtained by calcining $Pd/Al_2O_3$-EP to remove the residual carbon species was decreased to 130 °C.

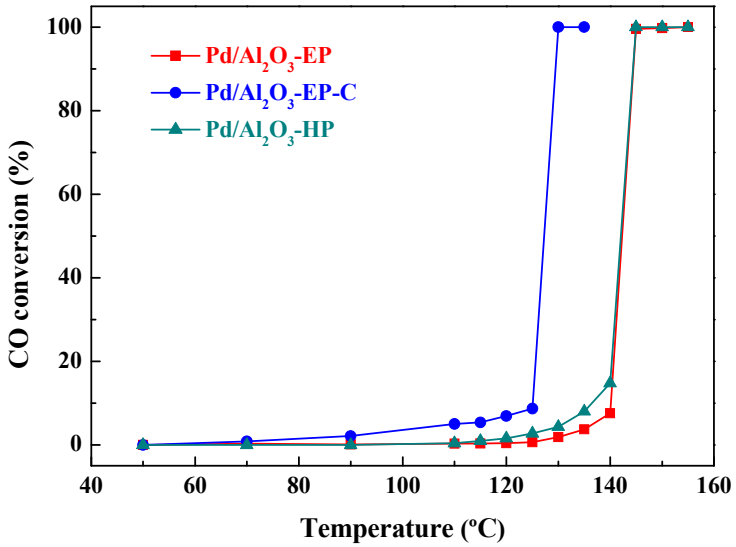


**Figure 4.** Catalytic activity of $Pd/Al_2O_3$-EP, $Pd/Al_2O_3$-EP-C, and $Pd/Al_2O_3$-HP catalysts for CO oxidation.

The particles size, oxidation state of the Pd species, and Pd/Al atomic ratios play important roles in CO oxidation. The particle size of the Pd species in $Pd/Al_2O_3$-EP-C (3.7 nm) is a little larger that in $Pd/Al_2O_3$-EP (3.2 nm) and $Pd/Al_2O_3$-HP (3.0 nm), which may decrease the CO oxidation

activity over $Pd/Al_2O_3$-EP-C to some extent. However, from the XPS data (Table 2), it can be seen that $Pd/Al_2O_3$-EP-C has the highest Pd/Al atomic ratio (0.0248), and the content of the active chemisorbed oxygen is as high as 46.9%. It proves that calcination can remove the residual carbon species that are produced from ethanol dissociation, and more active sites of Pd are exposed and more active chemisorbed oxygen species are generated. From Table 2, we can also see that more oxidative PdO are formed in comparison with $Pd/Al_2O_3$-EP and $Pd/Al_2O_3$-HP. Zhang et al. [36] claimed that PdO exihibits lower catalytic activity than metallic Pd due to the strong adsorption of CO molecules on PdO, which may inhibit the adsorption and activation of oxygen molecules. Luo et al. [37,38] investigated the performance of the PdO species on $CeO_2$ support and found that free surface PdO exhibited the highest catalytic activity for CO oxidation due to the synergistic effect of the free surface PdO species with the oxygen vacancies. In this work, the carbon species may facilitate the formation of the free surface PdO species in $Pd/Al_2O_3$-EP-C, which will be further investigated in the future. The synergistic effect of the free surface PdO species with the chemisorbed oxygen species may also enhance the performance of $Pd/Al_2O_3$-EP-C. Therefore, $Pd/Al_2O_3$-EP-C exhibits much higher CO oxidation performance than the other two $Pd/Al_2O_3$ samples. The $T_{100}$ of $Pd/Al_2O_3$-EP-C (130 °C) was much lower than the bimetallic $PdCu/Al_2O_3$-P catalyst that was prepared by AP hydrogen plasma (140 °C) [24], and the Pd/SBA-15 prepared by LP cold plasma [39].

## 3. Experimental

### *3.1. Materials*

The $Pd(NO_3)_2$ solution is a mixture of a certain proportion of $Pd(NO_3)_2{\cdot}H_2O$ and $HNO_3$ (Tianjin Kermel Chemical Reagent Co., Ltd., Tianjin, China.). The $\gamma$-$Al_2O_3$ (record as $Al_2O_3$, Qingdao Marine Chemical Plant, Qingdao, China) are 40–60 mesh pellets that were obtained by grinding and sieving. Before use, the $Al_2O_3$ pellets were calcined at 600 °C for 5 h. The $Pd/Al_2O_3$ precursor was prepared by an incipient wetness impregnation method, and the nominal concentrations of metal Pd was 2.0 wt % in this work.

### *3.2. Synthesis of $Pd/Al_2O_3$ Catalysts*

The $Pd/Al_2O_3$ catalysts were synthesized by a DBD cold plasma reactor at atmospheric pressure. The DBD reactor consists of a coaxial quartz tube with an inner diameter of 7.0 mm and an outer diameter of 10.0 mm, a copper inner electrode with a diameter of 2.0 mm, and an aluminum coil ground electrode. The discharge length and discharge gap were 25 mm and 2.5 mm, respectively. The sinusoidal AC power supply CTP-2000K (Nanjing Suman Electronic Co. Ltd., Nanjing, China) was used for power supply, and the discharge frequency and peak-to-peak voltage are maintained at 13.6 kHz and 19.2 kV, respectively.

The synthesis of $Pd/Al_2O_3$ catalysts using "storage-discharge" ethanol cold plasma method can be mainly divided into four steps, as shown in Scheme 1. Firstly, 0.3 g precursor of $Pd/Al_2O_3$ catalyst was put into the DBD reactor, and then ethanol was brought into the reactor by high-purity Ar for 10 min at a flow rate of 100 mL·min$^{-1}$ to adsorb ethanol molecules on the surface of $Al_2O_3$ support. Next, the DBD reactor was purged with Ar gas for 10 min at a flow rate of 100 mL·min$^{-1}$ to remove physically adsorbed ethanol molecules. Subsequently, the Pd precursor ions supported on the $Al_2O_3$ were reduced by cold plasma for 10 min with the assistance of the adsorbed ethanol molecules, and the obtained sample was recorded as $Pd/Al_2O_3$-EP. Finally, $Pd/Al_2O_3$-EP was calcined in an air atmosphere of 100 mL·min$^{-1}$ flow rate at 450 °C for 2 h to achieve the purpose of removing the residual carbon species dissociated from ethanol in the DBD cold plasma. The resulting sample was marked as $Pd/Al_2O_3$-EP-C. Hydrogen cold plasma was adopted to treat the freshly prepared $Pd/Al_2O_3$ for 10 min as a comparison, and the obtained catalyst was marked as $Pd/Al_2O_3$-HP. The working gas was a mixture of Ar and $H_2$ $\left(V_{H_2} : V_{Ar} = 1 : 1\right)$ with a flow rate of 100 mL·min$^{-1}$. As shown in Figure 5, the discharge powers of the "storage-discharge" ethanol cold plasma and hydrogen cold plasma, measured by the Lissajous figure

method using a 1000:1 P6015A high voltage probe with a capacitance of o.47 μF and a 10:1 N2862B voltage probe, were 2.3 W and 2.2 W, respectively.

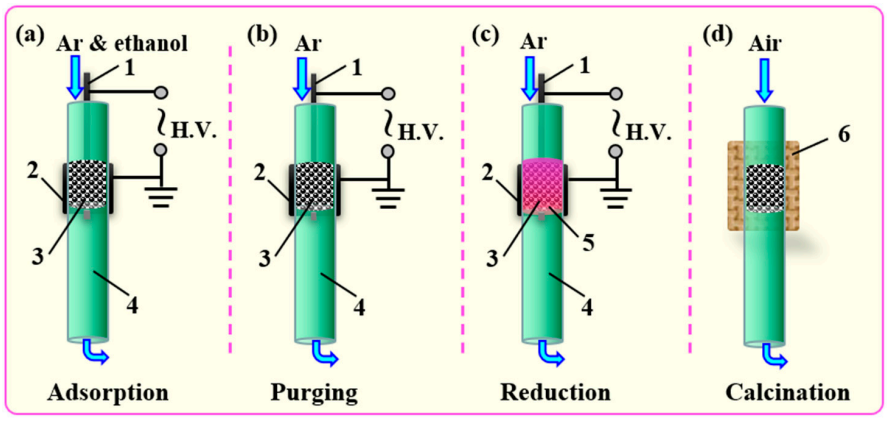


**Scheme 1.** Schematic diagram of $Pd/Al_2O_3$ catalysts synthesis using "storage-discharge" ethanol cold plasma: (**a**) Adsorption of ethanol; (**b**) Purging of the physically adsorbed ethanol; (**c**) Cold plasma reduction; (**d**) Removal of the residual carbon species by calcination. 1-inner electrode, 2-ground electrode, 3-catalyst, 4-quartz tube, 5-plasma zone, and 6-furance.

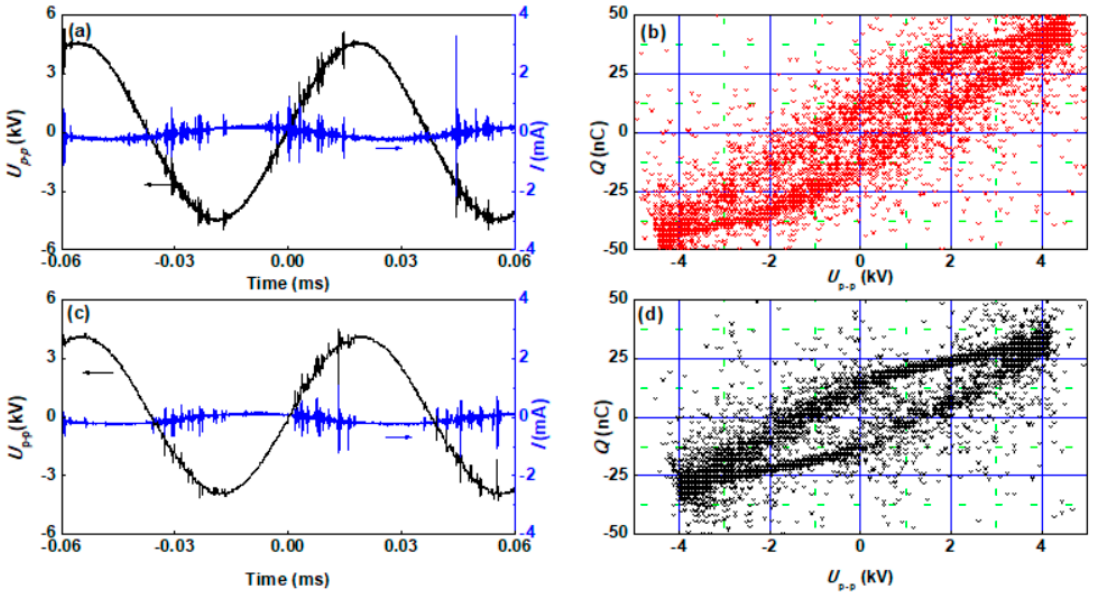


**Figure 5.** The discharge voltage and current waveforms, and the corresponding Lissajous figures of (**a**,**c**) the "storage-discharge" ethanol cold plasma and (**b**,**d**) hydrogen cold plasma for synthesis of $Pd/Al_2O_3$ catalysts.

### *3.3. Characterization*

The X-ray diffraction (XRD) characterization was performed on a DX-2700 (Dandong Haoyuan Instrument Co., Ltd., Dandong, China) diffractometer with Cu Kα radiation (λ = 0.154178 nm). The measured 2θ range was 10° to 80°, and the voltage and current are 40 kV and 30 mA, respectively. Using a Thermo VG ESCAL250 X-ray photoelectron spectrometer (Thermo VG Scientific, Waltham, MA, USA) that was equipped with Al Kα radiation (1486.6 eV) to perform X-ray photoelectron diffraction (XPS) on the surface chemical composition of the catalysts. The binding energies of the elements in the detection were calibrated by the orbital binding energy (284.6 eV) of C1s. Transmission electron microscopy (TEM) measurements were collected on a HT7700 transmission electron microscope (Hitachi, Ltd., Tokyo, Japan) with the acceleration voltage of 120 kV. Calculate the average size ($D_{mean}$) and corresponding size distribution of Pd nanoparticles by selecting more than 100 nanoparticles from the

TEM images. The characterization of $N_2$ adsorption/desorption was carried out on the NOVA 2200e gas sorption analyzer (Quantachrome Instruments, Boynton Beach, FL, USA). The Brunauer–Emmett–Teller (BET) specific surfaces areas ($S_{BET}$), pore volumes ($V_p$), and pore sizes ($D_p$) distributions of the samples were measured by $N_2$ adsorption/desorption. The adsorption and desorption data were analyzed using the Barrett–Joyner–Halenda (BJH) model and Halsey equations.

### *3.4. Activity Test*

The CO catalytic oxidation test was carried out in a quartz tube (inner diameter: 4.0 mm, outer diameter: 6.0 mm), and the mass of the $Pd/Al_2O_3$ sample used was 10 mg. The reaction with temperature range of 30–160 °C was performed under a stream of CO-$O_2$-$N_2$ mixture (1.0 vol% CO, 20.0 vol% $O_2$, and 79.0 vol% $N_2$) with the flow rate of 20 mL·min$^{-1}$. The SICK-MAIHAK S710 infrared absorption spectrometer (Sick-Maihak, Waldkirch, Germany) was used to determine the concentrations of CO and $CO_2$ in the outflow gas online.

## 4. Conclusions

In this work, a safe and efficient "storage-discharge" ethanol cold plasma method was successfully developed and applied to synthesize $Pd/Al_2O_3$ catalysts for CO oxidation. The results indicate that "storage-discharge" ethanol plasma has the ability to reduce Pd precursor ions to a metallic state, like hydrogen plasma, confirming that ethanol is an effective source for generating active hydrogen species. The CO catalytic oxidation performance for $Pd/Al_2O_3$-EP synthesized by the "storage-discharge" ethanol cold plasma is comparable to that for $Pd/Al_2O_3$-HP synthesized by the hydrogen cold plasma, and the $T_{100}$ is 145 °C. $Pd/Al_2O_3$-EP-C obtained by calcining $Pd/Al_2O_3$-EP to remove the residual carbon species shows much better CO oxidation performance, and the $T_{100}$ is 130 °C. It is mainly caused by the removal of the residual carbon species, and the exposure of more Pd active sites and active chemisorbed oxygen species. Meantime, the synergistic effect of the free surface PdO species with the chemisorbed oxygen species may also enhance the performance of $Pd/Al_2O_3$-EP-C.

The "storage-discharge" ethanol cold plasma method avoids the problem of extra residual carbon species being generated by the continuous discharge of ethanol plasma. It is a safe, efficient, and environmentally method to synthesize supported Pd catalysts and it possesses important potential application value for preparing other high performance supported metal catalysts.

**Supplementary Materials:** The following are available online at http://www.mdpi.com/2073-4344/10/8/907/s1, Figure S1: $N_2$ sorption isotherms (a) and pore size distributions (b) of $Pd/Al_2O_3$-EP, $Pd/Al_2O_3$-EP-C, $Pd/Al_2O_3$-HP, and the $Al_2O_3$ support, Figure S2: The TG and DTG curves of the $Pd/Al_2O_3$-EP catalyst in Ar atmosphere at a heating rate of 10 °C·min$^{-1}$.

**Author Contributions:** Conceptualization, L.D. and X.Z.; investigation, H.W. and Y.Z.; data curation, H.W. and T.Z.; writing—original draft preparation, H.W.; writing—review and editing, X.Z. and L.D.; supervision, L.D.; project administration, L.D. All authors have read and agreed to the published version of the manuscript.

**Funding:** This research was funded by National Natural Science Foundation of China (Grant No. 21773020, 21673026, 11505019), the Liaoning Innovative Talents in University (Grant No. LR2017025), the Natural Science Foundation of Liaoning Province (Grant No. 20180550085), the Graduate Education and Teaching Reform Fund of Dalian University, and Zhang Xiuling Innovation Studio of Dalian City.

**Conflicts of Interest:** The authors declare no conflict of interest.

## References

1. Di, L.B.; Li, Z.; Lee, B.; Park, D.W. An alternative atmospheric-pressure cold plasma method for synthesizing Pd/P25 catalysts with the assistance of ethanol. *Int. J. Hydrogen Energy* **2017**, *42*, 11372–11378. [CrossRef]
2. Di, L.B.; Zhang, X.L.; Xu, Z.J.; Wang, K. Atmospheric-pressure cold plasma for preparation of high performance $Pt/TiO_2$ photocatalyst and its mechanism. *Plasma Chem. Plasma Process.* **2013**, *34*, 301–311. [CrossRef]

3. Dao, V.D.; Choi, Y.; Yong, K.; Larina, L.L.; Shevaleevskiy, O.; Choi, H.S. A facile synthesis of bimetallic AuPt nanoparticles as a new transparent counter electrode for quantum-dot-sensitized solar cells. *J. Power Sources* **2015**, *274*, 831–838. [CrossRef]
4. Kim, T.; Lee, D.H.; Jo, S.; Pyun, S.H.; Kim, K.T.; Song, Y.H. Mechanism of the accelerated reduction of an oxidized metal catalyst under electric discharge. *ChemCatChem* **2016**, *8*, 685–689. [CrossRef]
5. Peng, H.; Ma, Y.; Liu, W.; Xu, X.; Fang, X.; Lian, J.; Wang, X.; Li, C.; Zhou, W.; Yuan, P. Methane dry reforming on $Ni/La_2Zr_2O_7$ treated by plasma in different atmospheres. *J. Energy Chem.* **2015**, *24*, 416–424. [CrossRef]
6. Li, Y.; Li, G.; Song, L.; Chu, W.; Dai, X.; Yin, Y. Modification of $Ni/SiO_2$ catalysts by means of a novel plasma technology. *Plasma Sci. Technol.* **2008**, *10*, 551–555.
7. Di, L.B.; Zhang, J.S.; Ma, C.; Tu, X.; Zhang, X.L. Atmospheric-pressure dielectric barrier discharge cold plasma for synthesizing high performance Pd/C formic acid dehydrogenation catalyst. *Catal. Today* **2019**, *337*, 201–207. [CrossRef]
8. Du, C.; Mo, J.; Tang, J.; Huang, D.; Mo, Z.; Wang, Q.; Ma, S.; Chen, Z. Plasma reforming of bio-ethanol for hydrogen rich gas production. *Appl. Energy* **2014**, *133*, 70–79. [CrossRef]
9. Greluk, M.; Slowik, G.; Rotko, M.; Machocki, A. Steam reforming and oxidative steam reforming of ethanol over $PtKCo/CeO_2$ catalyst. *Fuel* **2016**, *183*, 518–530. [CrossRef]
10. Bej, B.; Bepari, S.; Pradhan, N.C.; Neogi, S. Production of hydrogen by dry reforming of ethanol over alumina supported nano-$NiO/SiO_2$ catalyst. *Catal. Today* **2017**, *291*, 58–66. [CrossRef]
11. Spallina, V.; Matturro, G.; Ruocco, C.; Meloni, E.; Palma, V.; Fernandez, E.; Melendez, J.; Tanaka, A.P.; Sole, J.V.; Annaland, M.V.S.; et al. Direct route from ethanol to pure hydrogen through autothermal reforming in a membrane reactor: Experimental demonstration, reactor modelling and design. *Energy* **2018**, *143*, 666–681. [CrossRef]
12. Zhou, R.; Zhou, R.; Xian, Y.; Fang, Z.; Lu, X.; Bazaka, K.; Bogaerts, A.; Ostrikov, K. Plasma-enabled catalyst-free conversion of ethanol to hydrogen gas and carbon dots near room temperature. *Chem. Eng. J.* **2020**, *382*, 122745. [CrossRef]
13. Ulejczyk, B.; Nogal, L.; Mlotek, M.; Krawczyk, K. Hydrogen production from ethanol using dielectric barrier discharge. *Energy* **2019**, *174*, 261–268. [CrossRef]
14. Bardos, L.; Baránková, H.; Bardos, A. Production of hydrogen-rich synthesis gas by pulsed atmospheric plasma submerged in mixture of water with ethanol. *Plasma Chem. Plasma Process.* **2016**, *37*, 115–123. [CrossRef]
15. Xin, Y.; Sun, B.; Zhu, X.; Yan, Z.; Zhao, X.; Sun, X.; Ohshima, T. Characteristics and pathways of hydrogen produced by pulsed discharge in ethanol-water mixtures. *Int. J. Hydrogen Energy* **2020**, *45*, 1588–1596. [CrossRef]
16. Li, Z.; Zhang, J.S.; Wang, H.Y.; Li, Z.; Zhang, X.L.; Di, L.B. Preparation of Pd/C by atmospheric-pressure ethanol cold plasma and its preparation mechanism. *Nanomaterials* **2019**, *9*, 1437. [CrossRef]
17. Zhang, X.L.; Nie, L.H.; Xu, Y.; Shi, C.; Yang, X.F.; Zhu, A.M. Plasma oxidation for achieving supported $TiO_2$ photocatalysts derived from adsorbed $TiCl_4$ using dielectric barrier discharge. *J. Phys. D Appl. Phys.* **2007**, *40*, 1763–1768. [CrossRef]
18. Kim, H.H.; Oh, S.M.; Ogata, A.; Futamura, S. Decomposition of gas-phase benzene using plasma-driven catalyst (PDC) reactor packed with $Ag/TiO_2$ catalyst. *Appl. Catal. B Environ.* **2005**, *56*, 213–220. [CrossRef]
19. Van Durme, J.; Dewulf, J.; Leys, C.; Van Langenhove, H. Combining non-thermal plasma with heterogeneous catalysis in waste gas treatment: A review. *Appl. Catal. B Environ.* **2008**, *78*, 324–333. [CrossRef]
20. Kim, H.H.; Ogata, A.; Futamura, S. Oxygen partial pressure-dependent behavior of various catalysts for the total oxidation of VOCs using cycled system of adsorption and oxygen plasma. *Appl. Catal. B Environ.* **2008**, *79*, 356–367. [CrossRef]
21. Shi, C.; Chen, B.B.; Li, X.S.; Crocker, M.; Wang, Y.; Zhu, A.M. Catalytic formaldehyde removal by "storage-oxidation" cycling process over supported silver catalysts. *Chem. Eng. J.* **2012**, *200*, 729–737. [CrossRef]
22. Yao, X.; Gao, M.; Wei, Z.; Chen, M.; Shangguan, W. Removal of hexanal in cooking fume by combination of storage and plasma-catalytic oxidation on alkali-modified Co-Mn solid solution. *Chemosphere* **2019**, *220*, 738–747. [CrossRef]
23. Chen, B.; Wu, L.; Wu, B.; Wang, Z.; Yu, L.; Crocker, M.; Zhu, A.; Shi, C. Catalytic materials for low concentration VOCs removal through "storage-regeneration" cycling. *ChemCatChem* **2019**, *11*, 3646–3661. [CrossRef]

24. Di, L.B.; Duan, D.Z.; Park, D.W.; Ahn, W.S.; Lee, B.J.; Zhang, X.L. Cold plasma for synthesizing high performance bimetallic PdCu catalysts: Effect of reduction sequence and Pd/Cu atomic ratios. *Top. Catal.* **2017**, *60*, 925–933. [CrossRef]
25. Xu, W.J.; Zhan, Z.B.; Di, L.B.; Zhang, X.L. Enhanced activity for CO oxidation over $Pd/Al_2O_3$ catalysts prepared by atmospheric-pressure cold plasma. *Catal. Today* **2015**, *256*, 148–152. [CrossRef]
26. Di, L.B.; Xu, W.J.; Zhan, Z.B.; Zhang, X.L. Synthesis of alumina supported Pd-Cu alloy nanoparticles for CO oxidation via a fast and facile method. *RSC Adv.* **2015**, *5*, 71854–71858. [CrossRef]
27. Di, L.B.; Li, Z.; Zhang, X.L.; Wang, H.Y.; Fan, Z.Y. Reduction of supported metal ions by a safe atmospheric pressure alcohol cold plasma method. *Catal. Today* **2019**, *337*, 55–62. [CrossRef]
28. Vitiello, G.; Clarizia, L.; Abdelraheem, W.; Esposito, S.; Bonelli, B.; Ditaranto, N.; Vergara, A.; Nadagouda, M.; Dionysiou, D.D.; Andreozzi, R.; et al. Near UV-irradiation of $CuO_x$-impregnated $TiO_2$ providing active species for $H_2$ production through methanol photoreforming. *ChemCatChem* **2019**, *11*, 4314–4326. [CrossRef]
29. Baylet, A.; Marecot, P.; Duprez, D.; Castellazzi, P.; Groppi, G.; Forzatti, P. In situ Raman and in situ XRD analysis of PdO reduction and Pd degrees oxidation supported on gamma-$Al_2O_3$ catalyst under different atmospheres. *Phys. Chem. Chem. Phys.* **2011**, *13*, 4607–4613. [CrossRef]
30. Zhang, X.; Meng, J.; Zhu, B.; Yu, J.; Zou, S.; Zhang, Z.; Gao, Y.; Wang, Y. In situ TEM studies of the shape evolution of Pd nanocrystals under oxygen and hydrogen environments at atmospheric pressure. *Chem. Commun.* **2017**, *53*, 13213–13216. [CrossRef]
31. Qi, B.; Di, L.B.; Xu, W.J.; Zhang, X.L. Dry plasma reduction to prepare a high performance Pd/C catalyst at atmospheric pressure for CO oxidation. *J. Mater. Chem. A* **2014**, *2*, 11885–11890. [CrossRef]
32. Cui, W.; Li, S.; Wang, D.; Deng, Y.; Chen, Y. High reactivity and sintering resistance of $CH_4$ oxidation over modified $Pd/Al_2O_3$. *Catal. Commun.* **2019**, *119*, 86–90. [CrossRef]
33. Bi, Y.S.; Dang, G.Y.; Zhao, X.H.; Meng, X.F.; Lu, H.J.; Jin, J.T. Preparation, characterization and catalytic properties of Pd-Fe-zeolite and Pd-Ce-zeolite composite catalysts. *J. Hazard. Mater.* **2012**, *229*, 245–250. [CrossRef]
34. Wollbrink, A.; Volgmann, K.; Koch, J.; Kanthasamy, K.; Tegenkamp, C.; Li, Y.; Richter, H.; Kämnitz, S.; Steinbach, F.; Feldhoff, A.; et al. Amorphous, turbostratic and crystalline carbon membranes with hydrogen selectivity. *Carbon* **2016**, *106*, 93–105. [CrossRef]
35. Zhao, X.; Zhua, H.; Yang, X. Amorphous carbon supported $MoS_2$ nanosheets as effective catalysts for electrocatalytic hydrogen evolution. *Nanoscale* **2014**, *6*, 10680–10685. [CrossRef]
36. Zhang, Y.; Cai, Y.; Guo, Y.; Wang, H.; Wang, L.; Lou, Y.; Guo, Y.; Lu, G.; Wang, Y. The effects of the Pd chemical state on the activity of $Pd/Al_2O_3$ catalysts in CO oxidation. *Catal. Sci. Technol.* **2014**, *4*, 3973–3980. [CrossRef]
37. Meng, L.; Jia, A.P.; Lu, J.Q.; Luo, L.F.; Huang, W.X.; Luo, M.F. Synergetic effects of PdO species on CO oxidation over PdO–$CeO_2$ catalysts. *J. Phys. Chem. C* **2011**, *115*, 19789–19796. [CrossRef]
38. Wang, S.Y.; Li, N.; Zhou, R.M.; Jin, L.Y.; Hu, G.S.; Lu, J.Q.; Luo, M.F. Comparing the CO oxidation activity of free PdO and $Pd^{2+}$ ions over PdO-$CeO_2/SiO_2$ catalysts. *J. Mol. Catal. A Chem.* **2013**, *374–375*, 53–58. [CrossRef]
39. Wang, H.; Liu, C.J. Preparation and characterization of SBA-15 supported Pd catalyst for CO oxidation. *Appl. Catal. B Environ.* **2011**, *106*, 672–680. [CrossRef]